Optics and Laser Technology 131 (2020) 106410

Contents lists available at ScienceDirect

Optics and Laser Technology

journal homepage: www.elsevier.com/locate/optlastec

Full length article

Subsurface defect detection using phase evolution of line laser-generated Rayleigh waves

Dan Chen[a,b,c,1], Gaolong Lv[a,b,c,1], Shifeng Guo[a,b,c,*], Rui Zuo[a,b,c], Yanjun Liu[d], Kaixing Zhang[e], Zhongqing Su[f], Wei Feng[a,b,c]

[a] Shenzhen Key Laboratory of Smart Sensing and Intelligent Systems, Shenzhen Institutes of Advanced Technology, Chinese Academy of Sciences, Shenzhen 518055, China
[b] Guangdong Provincial Key Lab of Robotics and Intelligent System, Shenzhen Institutes of Advanced Technology, Chinese Academy of Sciences, Shenzhen 518055, China
[c] CAS Key Laboratory of Human-Machine Intelligence-Synergy Systems, Shenzhen Institutes of Advanced Technology, Shenzhen 518055, China
[d] Department of Electrical and Electronic Engineering, Southern University of Science and Technology, Shenzhen 518055, China
[e] College of Mechanical and Electronic Engineering, Shandong Agricultural University, Tai'an 271018, China
[f] Department of Mechanical Engineering, The Hong Kong Polytechnic University, Hung Hom, Kowloon 999077, Hong Kong Special Administrative Region

HIGHLIGHTS

- Phase evolution of Rayleigh ultrasonic waves is reported to detect subsurface defects.
- The mechanisms of phase evolution with defect width and depth are intensively studied.
- The relationships between phase evolution and defect width and depth are established.
- A sensitive and robust parameter is proposed to detect and quantify subsurface defect.

ARTICLE INFO

Keywords:
Rayleigh wave
Laser ultrasonics
Subsurface defects
Phase evolution
Nondestructive evaluation

ABSTRACT

An unreported phenomenon of phase evolution of Rayleigh ultrasonic waves with subsurface defects is observed and systematically explored for detection of subsurface defects using non-contact line laser ultrasonic technique and numerical simulation. The mechanism of phase evolution of Rayleigh wave signals is explained by the interference of the reflected and direct Rayleigh wave, explored by finite element analysis. Both experiments and simulation show distinct peak evolution of the Rayleigh wave signals with the width and depth of subsurface defect. A dimensionless parameter (|Neg|/Pos), defined by the ratio of absolute negative peak to positive peak of Rayleigh wave, is proposed to evaluate the phase evolution of Rayleigh wave with defect width and depth, which is further used to quantify the subsurface defects. The phase evolution of Rayleigh waves can act as a robust and sensitive feature to detect subsurface defects using laser-generated ultrasound, which has promising applications in life prediction and health monitoring of various engineering structures.

1. Introduction

The subsurface defect hidden beneath the surface of structure is detrimental to the strength, performance and lifetime of critical structure and may cause catastrophic accidents if not detected in advance [1–3]. In particular, for the additive manufactured structures, the interlayer defects, such as pores, inclusions and cracks, are inevitably introduced and difficult to be detected in-situ by conventional detection methods [4–6]. A reliable nondestructive evaluation (NDE) technique that enables the detection and evaluation of subsurface defects in safety-critical structures is therefore highly demanded. Ultrasonic inspection has received considerable attention for identifying internal and subsurface defects of various structures [7–10]. However, conventional ultrasonic NDE techniques are generally contact-based and require additional coupling agent, fixtures for generation and detection of ultrasonic signals [11–18], which are not applicable in harsh environment (high temperature, serious radiation, etc.) and for complicated structures.

* Corresponding author at: Shenzhen Key Laboratory of Smart Sensing and Intelligent Systems, Shenzhen Institutes of Advanced Technology, Chinese Academy of Sciences, Shenzhen 518055, China.
E-mail address: sf.guo@siat.ac.cn (S. Guo).
[1] The authors contributed equally to this work.

https://doi.org/10.1016/j.optlastec.2020.106410
Received 22 March 2020; Received in revised form 17 May 2020; Accepted 4 June 2020

Laser ultrasound (LU) is a technique that based on thermoelastic or ablation mechanism to generate ultrasonic waves and using interferometer to detect surface displacement of structures [19–21]. LU with the advantages of non-contact generation and detection, broad bandwidth reception, accessibility for harsh environments and complex structures, has been implemented for inspecting structural materials with various defects [20,22–25]. The laser generated Rayleigh waves that propagate along the surface of structures are more sensitive to detect surface-breaking cracks or subsurface defects than bulk longitudinal wave and shear wave [26–29].

The interaction of laser-generated Rayleigh waves with surface-breaking cracks has been studied using theoretical model [20], numerical simulation and scanning laser source technique [30]. By analyzing the features of velocity dispersion [31], time-of-flight, time-domain signal amplitude, and spectrum distribution of the laser generated Rayleigh waves, the internal or subsurface defects can be detected [32]. However, the above mentioned laser ultrasonic methods have limitations in low detection sensitivity, weak robustness, and require reference parameters for comparison, therefore are difficult to be applied in real applications.

This paper presents a systematic study of the interaction of line laser-generated Rayleigh waves with subsurface defects, and a new method to detect subsurface defects is proposed. The phase evolution, an unreported phenomenon, which shows the transformation of Rayleigh wave peak with the presence of subsurface defects are explored experimentally and numerically. A dimensionless parameter |Neg|/Pos is proposed to quantitatively describe the relationship between phase evolution and defect depth and width. The phase evolution of Rayleigh waveforms can be adopted as a reliable and sensitive feature to evaluate and monitor the structure integrity.

2. Pulsed-laser ultrasonic experiment

2.1. Experimental details

The experimental setup is shown in Fig. 1(a). A Nd: YAG pulsed laser (Centurion +) with wavelength of 1064 nm, pulse duration of 12 ns is used to generate Rayleigh wave. The pulsed laser is focused as a line source with length of 15 mm and width of 0.5 mm. The double-wave mixed interferometer (TEMPO 2D, Sound & Bright company, USA) with an operating wavelength of 532 nm and a bandwidth of 20 MHz is applied to receive the Rayleigh ultrasonic waves. A band-pass filter of 532 nm is placed in front of the interferometer lens to avoid the generation of disturbance signal by the pulsed laser. The stainless steel (316 L) plates measuring 60 mm in length, 10 mm in thickness and 40 mm in width, with various artificial subsurface defects, are investigated. The energy of each pulsed laser is limited to 5 mJ, and the corresponding energy density for the given line laser source is estimated at 66.7 mJ/cm^2, which is significantly lower than the ablation threshold of the stainless steel [33]. For defects with sizes much smaller than the line laser source and far away from the detection point, the effect of orientation and shape of defects on the received Rayleigh wave signals can be ignored [34]. For simplicity, a series of rectangular-shape slits (ARSSs) of fixed height (H) of 1.0 mm, varying depth (D) of 0.5, 1.0, 1.5 mm and various width (W) of 0, 0.5, 1.5, 3 mm, are therefore fabricated as subsurface defects in specimen.

Both the excitation laser source and the detection laser source are kept at 5 mm away from the center of defects, with a distance of 10 mm in x direction for all specimens. The acquired signals are digitized by a high-resolution data acquisition card (DAC) [Fig. 1(b)], and averaged 200 times to improve the signal-to-noise ratio. To exclude any effect from surface roughness, the front surface of all specimens is milled to about 0.8 μm. The representative time-domain signal from defect-free specimen is shown in Fig. 2(a). Three type of waveforms, including, skimming longitudinal wave (SL), Rayleigh wave (R) and reflected longitudinal wave (L_r) from the bottom of specimen are identified by the calculated wave velocity. It can be seen in Fig. 2(a) that the Rayleigh wave free of defect is mainly manifested as an obvious negative monopolar signal with a significant negative peak and a high signal-to-noise ratio. The disturbance signal (DS) is attributed to the system interference.

Fig. 2(b) shows ten signals obtained from different positions along the y-axis, with fixed ARSS dimension H, D, W of 1.0, 0.5, and 1.5 mm, respectively. The zoomed Rayleigh waves in Fig. 2(c) show that the ten signals have excellent in consistency, indicating the received signal is stable and unaffected by the signal acquisition position. The representative frequency spectrum of Rayleigh wave signal is shown in Fig. 2(d). The central frequency of the generated Rayleigh wave is around 3.0 MHz, and the acoustic energy is mainly concentrated in the range of 2–4.5 MHz, with the estimated wavelength from 0.84 to 1.9 mm.

To study the interaction of Rayleigh waves with subsurface defects, a series of specimens with ARSSs at a fixed defect width (W) of 1.0 mm and various depths (D) of 0.5, 1.0, 1.5 mm are prepared for experiment. For specimen free of subsurface defect, a strong negative peak is observed (pointed by green arrow), with a negligible positive peak (pointed by red arrow), shown in Fig. 3(a). With the occurrence of an ARSS with depth (D) of 0.5 mm, a strong positive peak occurs, shown in Fig. 3(b). However, the positive peak decreases when the depth of ARSS increases to 1.0 mm, and it reduces substantially as the depth increased to 1.5 mm, shown in Fig. 3(c-d). In contrast, the negative peak deceases at defect depth of 0.5 mm but increases with defect depth increases. The result indicates that the phase evolution of Rayleigh waves (an obvious positive peak) can act as a robust and sensitive feature to detect subsurface defects. The reason for the evolved positive peak with defect depth will be further analyzed by finite element simulation in the

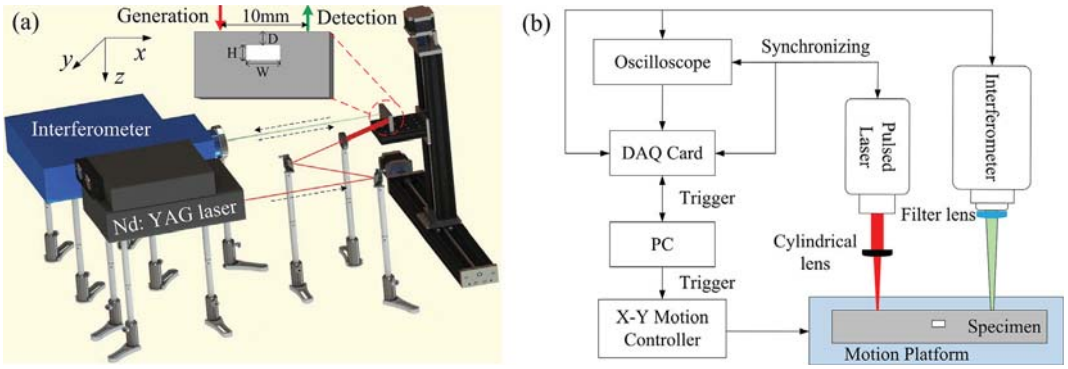

Fig. 1. Schematic diagram of laser ultrasonic experiment for detection of subsurface defects in stainless steel. (a) The configuration of experimental setup. H, D and W are abbreviations of the height, depth and width of subsurface defect, respectively. (b) The schematic of the experimental setup for detecting subsurface defects using Rayleigh waves excited by a pulsed laser and detected by a double-wave mixed interferometer.

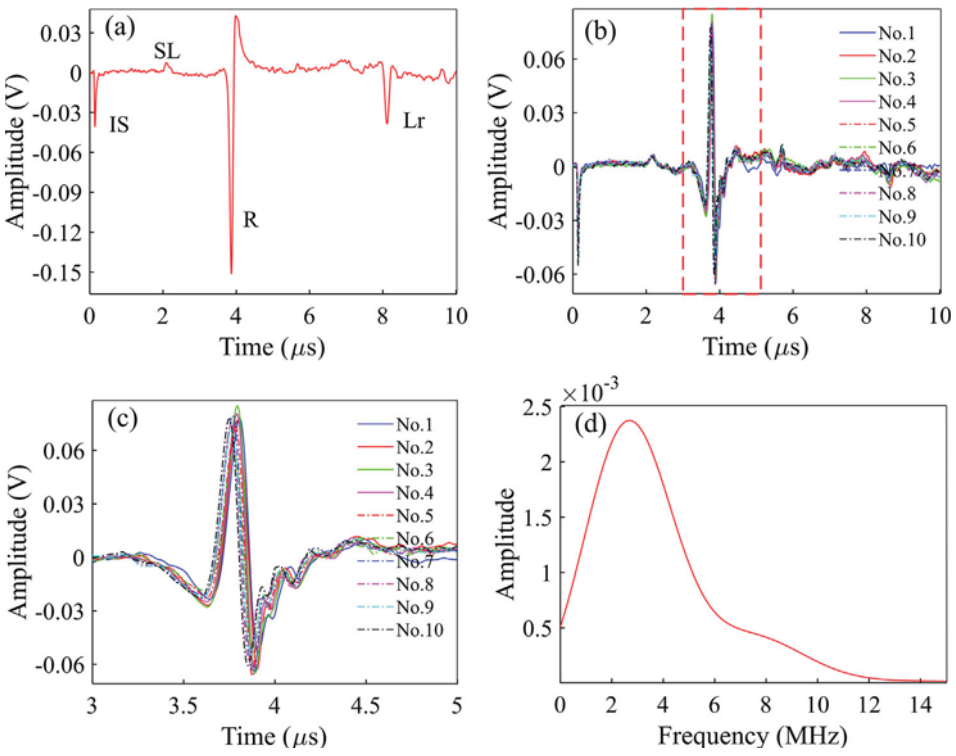

Fig. 2. The representative Rayleigh ultrasonic waves from (a) Specimen without defect, DS, SL, R and Lr are abbreviations of disturbance signal, skimming longitudinal wave, Rayleigh wave, and reflected longitudinal wave, respectively. (b) Specimen with defect dimension H, D, W of 1.0, 0.5 and 1.5 mm, obtained from 10 different positions along the y-axis. (c) The zoomed signals in (b) (identified by the dash line box). (d) The representative frequency spectrum of the Rayleigh wave from (c).

following section. In addition, it should be pointed out that the phase evolution of Rayleigh waves with subsurface defects is unique in line laser source generation and interferometer reception, which is not feasible to be observed using piezoelectric ultrasonic transducers, due to their bandwidth limitations [10,14]. Compared with the piezoelectric ultrasonic transducers, the laser interferometer has broader bandwidth and the out-of-plane displacement can be only detected, which enables it to separate the phase differences in signal. In addition, according to the Huygens principle, Rayleigh waves generated by a line laser source can be regarded as superposition of a series of spherical wave fronts in the propagation direction, which ensures the generated negative-going monopolar Rayleigh wave signal having a higher signal-to-noise ratio and better directivity than a point laser source under the same radiated power density[36], consequently facilitating to generate phase evolution.

2.2. Numerical simulation and analysis

In order to explain the phenomenon of phase evolution of Rayleigh wave, a two-dimensional finite element model is established using Comsol Multiphysics 5.4. The thermal stress module is selected to model the interaction of Rayleigh waves with subsurface defects. The governing equations for the coupled temperature and displacement fields is expressed as [35]

$$\nabla^2 T - \frac{1}{\kappa}\dot{T} - \frac{1}{c^2}\ddot{T} = -\frac{q}{k} \tag{1}$$

and

$$\mu\nabla^2 u + (\lambda + \mu)\nabla(\nabla \cdot u) = \rho\ddot{u} + \beta\nabla T \tag{2}$$

where T is the absolute temperature, $\mathbf{u}$ the displacement vector field, κ the thermal diffusivity, c the heat propagation speed that is equal to the longitudinal wave speed, k the thermal conductivity, β the thermoacoustic coupling constant: $\beta = (3\lambda + 2\mu)\alpha_T$, λ, μ the Lamé constant, α_T the coefficient of the linear thermal expansion. q is the heat source due to laser line-source illumination, which has a Gaussian distribution in x-z plane. The heat flow that has the same parameters as the pulsed laser energy is applied to the top boundary of the model. The heat flow function is expressed as

$$q = P_0(1 - r)\frac{t}{\tau}\exp\left(-\frac{x^2}{\delta^2}\right)\exp\left(-\frac{t}{\tau}\right) \tag{3}$$

where P_0 is the power amplitude, r the light reflection coefficient, τ and δ the rise time and line width of the pulsed laser. In addition, low-reflection boundaries are considered on both sides of the model and local mesh refinement is conducted on the top boundary. To observe the

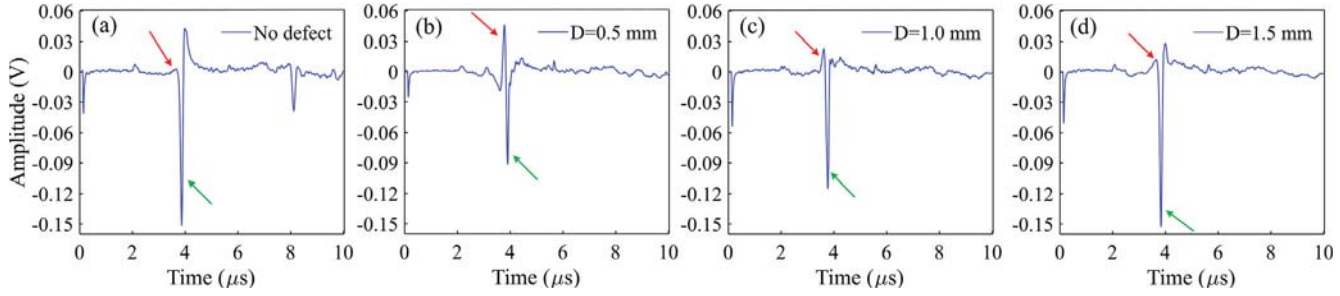

Fig. 3. Phase evolution of Rayleigh wave with defect depth. (a) Without defect. (b-d) Subsurface defects with depth of 0.5, 1.0, 1.5 mm. The height (H) and width (W) of the defect are 1.0 mm.

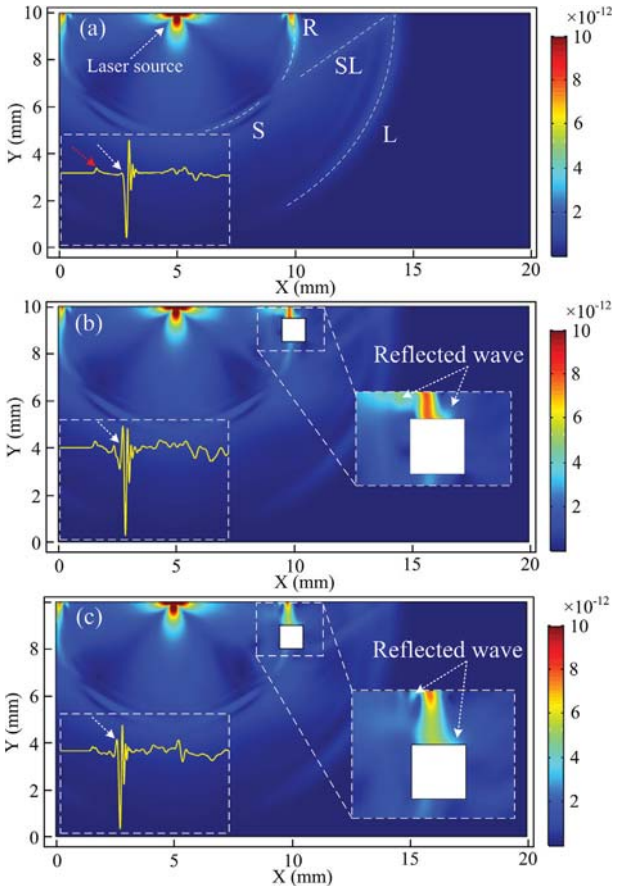

Fig. 4. The total displacement field simulated in specimens with and without defects. (a) Without defect. (b) Defect depth of 0.5 mm. (c) Defect depth of 1.0 mm. The simulated time-domain signals and the displacement field at each depth are inserted. The height (H) and Width (W) of the defect is kept at 1.0 and 1.0 mm, respectively.

wave propagation and interaction between the generated ultrasonic waves and defects, the model is solved using transient solver.

Fig. 4 shows the total displacement field simulated in specimens without and with various defect depths. Four types of waveforms, including the Rayleigh wave (R), shear wave (S), skimming longitudinal wave (SL) and body longitudinal wave (L), are clearly identified by the propagation direction and wave velocity, shown in Fig. 4(a). For the specimen free of defect, the Rayleigh wave has the strongest magnitude compared with other waveforms and mainly concentrated in the depth less than 2 mm. For comparison, the y-axis displacement serial that corresponding to the out-plane displacement in experiment are inserted in each subplot. The Rayleigh wave and skimming longitudinal wave are marked with red and white arrows in inserted waveform in Fig. 4(a).

For the subsurface defect with depth (D) of 0.5 mm, an enhanced Rayleigh wave is observed, shown in Fig. 4(b), which is mainly attributed to the superimposition of the reflected and direct Rayleigh waves with wavelength larger than 0.5 mm. The presence of the subsurface defect generates a strong positive peak, pointed by the white arrow in inset, which is consistent with the experimental results in Fig. 3(b). The phase evolution as a result of the subsurface defect can be explained by the interference of direct and reflected Rayleigh wave, which can act as an obvious indicator for the presence of subsurface defect. The phase change of Rayleigh wave has also been studied to detect surface crack [36], but which is generated mainly by the interaction of near-field surface wave and bulk wave between the laser source and the defect. Therefore, such method is only applicable to detect localized surface-breaking defects, with limited applications.

As the energy of Rayleigh wave decays exponentially with depth, the reflected Rayleigh wave substantially reduces when the defect depth increases to 1.0 mm. Therefore, the superimposition of reflected and direct Rayleigh waves is reduced [Fig. 4(c)], consequently with a reduced positive peak, shown in inset of Fig. 4(c). The simulation result is consistent well with the experimental result in Fig. 3. Both show a strong evolved positive peak of Rayleigh wave signals at small defect depth of 0.5 mm and a reduced positive peak with larger defect depth.

3. Results and discussions

The phase evolution of Rayleigh wave with defect width is further explored, conducted on specimens with fixed defect depth (0.5 mm) and various defect width (0, 0.5, 1.5, and 3 mm). The result in Fig. 5 shows that the evolution of positive peak of Rayleigh wave occurs at defect width of 0.5 mm, and the positive peak increases obviously with defect width increases, identified by the red arrow, with the value increases linearly from 0 to 0.12 V, summarized in Fig. 6. The negative peak of the Rayleigh wave (pointed by green arrow), however, decreases monotonically with defect width increases, with the value decreases linearly from 0.15 to 0 V. This result shows that the phase evolution of Rayleigh wave is extremely sensitive to the width of subsurface defects.

The pulse duration of Rayleigh wave in Fig. 2(c) is estimated as 1 μs. As the velocity of Rayleigh wave is about 3000 m/s, the length of the generated Rayleigh wave along the propagation direction is estimated at 3 mm. Therefore, for defect with width of 0.5 mm, part of the reflected Rayleigh wave dissipates during propagation (shown in Fig. 4(b)), and such dissipation effects is reduced with defect width increases and therefore induces a stronger superimposition of the reflected and direct Rayleigh wave. This may explain the evolved positive peak of the Rayleigh waves is weaker at small defect width and increases with defect width increases. The result in Figs. 5 and 6 show that the phase of Rayleigh wave changes obviously and monotonically as defect width, suggesting it can be used as a reliable indicator for measuring the width of subsurface defects. In addition, the normalized spectrum of the transmitted Rayleigh wave with the width of subsurface defects is analyzed, shown in Fig. 7. The result indicates that both the central frequency and bandwidth of the Rayleigh waves are not substantially affected by the width of subsurface defects.

In order to obtain a general relationship of phase evolution of Rayleigh wave with defect depth and width, specimens with various

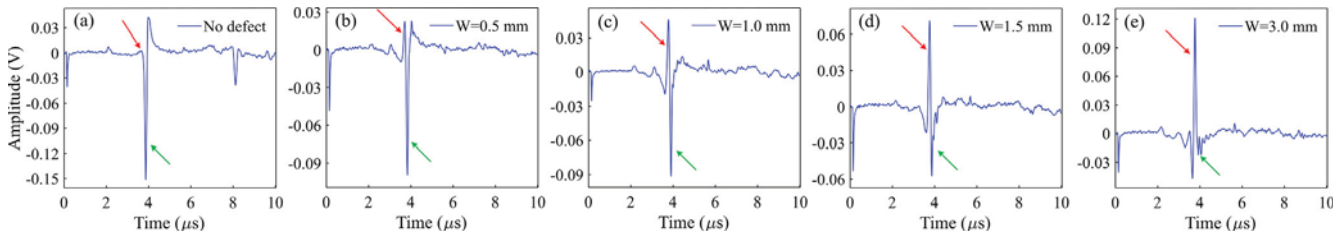

Fig. 5. Phase evolution of Rayleigh wave with defect depth. (a) Without defect. (b) Defect width of 0.5 mm. (c-e). Defect width of 1.0, 1.5, 3.0 mm. The height (H) and depth (D) is fixed at 1.0 mm and 0.5 mm, respectively.

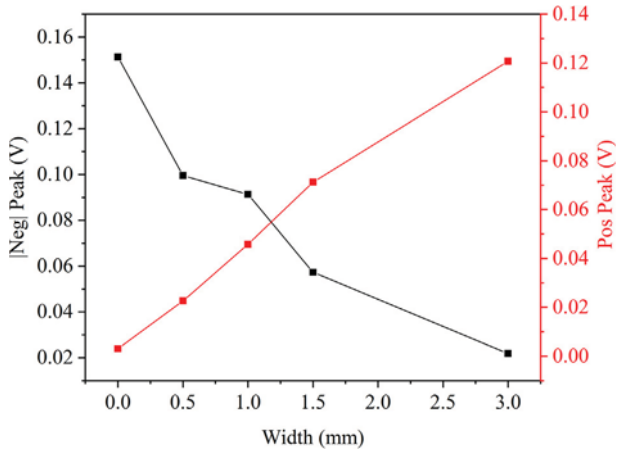

Fig. 6. Variation of the |Neg| peak and positive peak of the Rayleigh wave with subsurface defect width.

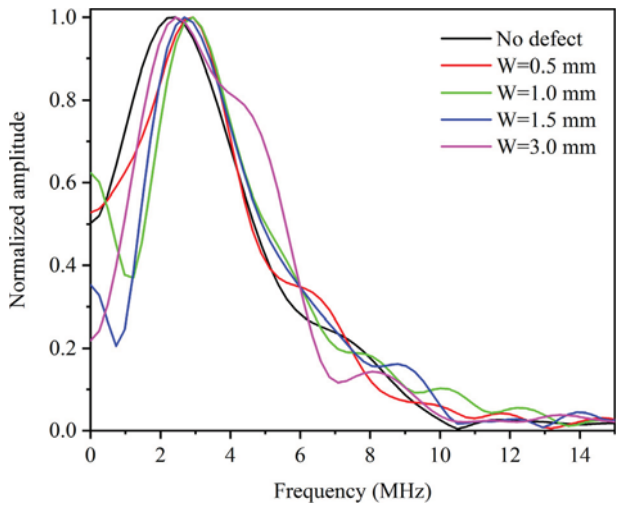

Fig. 7. Normalized spectrum of the transmitted Rayleigh wave with different widths of subsurface defects.

depths (0.5, 1.0, 1.5 mm) and widths (0.5, 0.8, 1.0, 1.2, 1.5, 2.0, 3.0 mm) are detected, with a total number of 21 specimens. Three characteristic parameters, including the absolute negative peak (|Neg| peak), positive peak (Pos-peak), and ratio of absolute negative peak to positive peak (|Neg|/Pos), are proposed to describe the phase evolution of Rayleigh wave. Fig. 8(a) shows the relationship between Neg-peak and the defect width and depth. At the fixed defect depth of 0.5 mm, the absolute value of Neg-peak (|Neg| peak) decreases monotonically with defect width increases. However, for defect depth of 1.0 and 1.5 mm, the |Neg| peak does not change substantially with defect width.

Fig. 8(b) shows the relationship between the Pos-peak and defect width and depth. In contrast, the Pos-peak value exhibits a completely opposite trend to that of in Fig. 8(a), which increases monotonically with defect width increases. According to the numerical simulation results in Fig. 4, the difference in the slope of |Neg|-peak curve [Fig. 8(a)] and Pos-peak curve [Fig. 8(b)] with defect depth is attributed to the penetration depth of the Rayleigh wave. While the difference in the slope of |Neg|-peak curve and Pos-peak curve changed with defect width is attributed to the length of Rayleigh waves. The comparison between Fig. 8(a) and (b) shows the transformation between the negative peak and positive peak of Rayleigh wave, which undoubtedly proves the occurrence of phase evolution and implies the existence of subsurface defects.

The |Neg|/Pos proposed is a dimensionless parameter that eliminates the impact of incident laser energy, material attenuation, and propagation distance on the amplitude of Rayleigh wave. As shown in Fig. 8(c), the |Neg|/Pos parameter decreases monotonically with defect width increases at evaluated defect depths for three defect depths. Therefore the |Neg|/Pos parameter can be acted as an important parameter to quantify the width and depth of the subsurface defects.

4. Conclusion

An unreported phenomenon of phase evolution of Rayleigh waves with subsurface defects is observed and systematically explored using all-optical laser ultrasonic experiment and numerical simulation. The phase evolution or even reversal of the Rayleigh wave is attributed to the superposition of the reflected Rayleigh wave and the direct Rayleigh wave with wavelength larger than the defect depth. A dimensionless parameter |Neg|/Pos is proposed to evaluate the phase evolution of Rayleigh wave quantitatively, which presents a monotonically variation trends with defect width and depth. Therefore, |Neg|/Pos can be used as a reliable parameter to quantify the depth and width of subsurface defects. In further work, we will consider to use the transient gating technique to excite single frequency Rayleigh waves, which enable to provide more precise indication of the subsurface defect characteristics.

5. Author statement

Shifeng Guo supervised the project, conceived the approach, evaluate the results and corrected the manuscript. Dan Chen implemented the experiments, analyzed the data and wrote the paper. Gaolong Lv prepared and carried out the experiments. Rui Zuo prepared the experimental setup. Yanjun Liu guided the laser ultrasonic experiments. Wei Feng, Kaixing Zhang, and Zhongqing Su evaluated and commented on the results. Dan Chen and Gaolong Lv contributed equally to this work.

Declaration of Competing Interest

None.

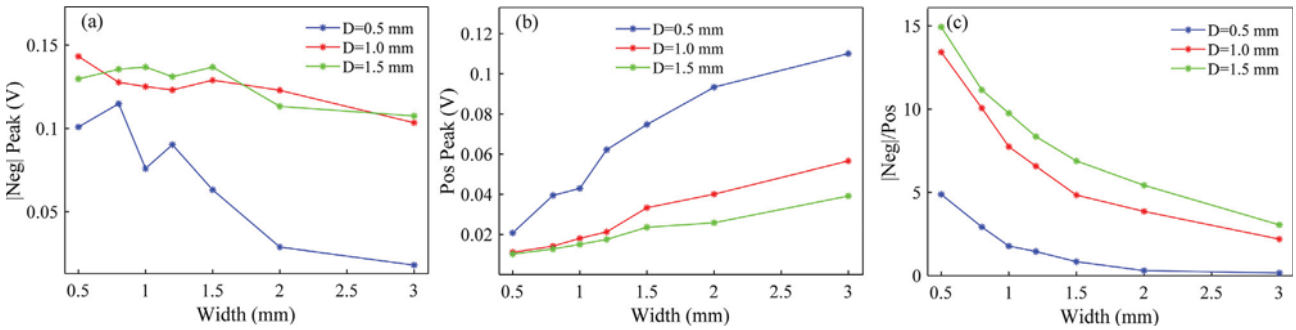

Fig. 8. The relationships between characteristic parameters and defect depth and width. (a) |Neg|-peak. (b) Pos-peak. (c) |Neg|/Pos.

Acknowledgements

The authors are grateful to the financial support from the National Natural Science Foundation of Guangdong (grant numbers 2016A030313177), Guangdong Frontier and Key Technological Innovation (grant numbers 2017B090910013), Science and Technology Innovation Commission of Shenzhen (grant numbers ZDSYS20190902093209795, JCYJ20170818153048647 and JCYJ20180507182239617).

Appendix A. Supplementary material

Supplementary data to this article can be found online at https://doi.org/10.1016/j.optlastec.2020.106410.

References

[1] P. Maruschak, O. Prentkovskis, R. Bishchak, Defectiveness of external and internal surfaces of the main oil and gas pipelines after long-term operation, J. Civil Eng. Manage. 22 (2) (2016) 279–286.
[2] J. Wu, J. Zhu, H. Xia, C. Liu, X. Huang, G.Y. Tian, DC-biased magnetization based eddy current thermography for subsurface defect detection, IEEE Trans. Ind. Inf. 15 (12) (2019) 6252–6259.
[3] J. Ahmad, A. Akula, R. Mulaveesala, H. Sardana, An independent component analysis based approach for frequency modulated thermal wave imaging for subsurface defect detection in steel sample, Infrared Phys. Technol. 98 (2019) 45–54.
[4] S.K. Everton, M. Hirsch, P. Stravroulakis, R.K. Leach, A.T. Clare, Review of in-situ process monitoring and in-situ metrology for metal additive manufacturing, Mater. Des. 95 (2016) 431–445.
[5] D. Cerniglia, M. Scafidi, A. Pantano, J. Rudlin, Inspection of additive-manufactured layered components, Ultrasonics 62 (2015) 292–298.
[6] C. Millon, A. Vanhoye, A.-F. Obaton, J.W. Penot, Development of laser ultrasonics inspection for online monitoring of additive manufacturing, Weld. World 62 (3) (2018) 653–661.
[7] H. Xiao, D. Chen, J. Xu, S. Guo, Defects identification using the improved ultrasonic measurement model and support vector machines, NDT and E Int. 111 (2020) 1–9.
[8] V. Zarubin, A. Bychkov, V. Simonova, V. Zhigarkov, A. Karabutov, E. Cherepetskaya, A refraction-corrected tomographic algorithm for immersion laser-ultrasonic imaging of solids with piecewise linear surface profile, Appl. Phys. Lett. 112 (21) (2018) 1–5.
[9] D. Chen, H. Xiao, M. Li, J. Xu, A study on the inclusion sizing using immersion ultrasonic C-scan imaging, J. Phys.: Conf. Ser., IOP Publish. 842 (1) (2017) 1–7.
[10] S. Guo, L. Zhang, S. Chen, C.K.I. Tan, K. Yao, Ultrasonic transducers from thermal sprayed lead-free piezoelectric ceramic coatings for in-situ structural monitoring for pipelines, Smart Mater. Struct. 28 (7) (2019) 1–9.
[11] S. Guo, S. Chen, L. Zhang, Y.F. Chen, K. Yao, Plastic strain determination with nonlinear ultrasonic waves using in situ integrated piezoelectric ultrasonic transducers, IEEE Trans. Ultrason. Ferroelectr. Freq. Control 65 (1) (2018) 95–101.
[12] S. Guo, L. Zhang, M.S. Mirshekarloo, S. Chen, Y.F. Chen, Z.Z. Wong, Z. Shen, H. Liu, K. Yao, Method and analysis for determining yielding of titanium alloy with nonlinear Rayleigh surface waves, Mater. Sci. Eng., A 669 (2016) 41–47.
[13] D. Chen, H. Xiao, J. Xu, An improved Richardson-Lucy iterative algorithm for C-scan image restoration and inclusion size measurement, Ultrasonics 91 (2019) 103–113.
[14] S. Guo, S. Chen, L. Zhang, W.H. Liew, K. Yao, Direct-write piezoelectric ultrasonic transducers for pipe structural health monitoring, NDT and E Int. 107 (2019) 1–7.
[15] Y. Lu, L. Ye, Z. Su, Crack identification in aluminium plates using Lamb wave signals of a PZT sensor network, Smart Mater. Struct. 15 (3) (2006) 839–849.
[16] X. Zhao, H. Gao, G. Zhang, B. Ayhan, F. Yan, C. Kwan, J.L. Rose, Active health monitoring of an aircraft wing with embedded piezoelectric sensor/actuator network: I. Defect detection, localization and growth monitoring, Smart Mater. Struct. 16 (4) (2007) 1–10.
[17] M. Li, X. Li, C. Gao, Y. Song, Acoustic microscopy signal processing method for detecting near-surface defects in metal materials, NDT and E Int. 103 (2019) 130–144.
[18] Z. Zhang, S. Guo, Q. Li, F. Cui, A.A. Malcolm, Z. Su, M. Liu, Ultrasonic detection and characterization of delamination and rich resin in thick composites with waviness, Compos. Sci. Technol. 189 (2020) 1–11.
[19] J. Herrmann, J.Y. Kim, L.J. Jacobs, J. Qu, J.W. Littles, M.F. Savage, Assessment of material damage in a nickel-base superalloy using nonlinear Rayleigh surface waves, J. Appl. Phys. 99 (12) (2006) 1–8.
[20] Z. Zhou, K. Zhang, J. Zhou, G. Sun, J. Wang, Application of laser ultrasonic technique for non-contact detection of structural surface-breaking cracks, Opt. Laser Technol. 73 (2015) 173–178.
[21] M. Duquennoy, M. Ouaftouh, J. Deboucq, J.-E. Lefebvre, F. Jenot, M. Ourak, Influence of a superficial field of residual stress on the propagation of surface waves—Applied to the estimation of the depth of the superficial stressed zone, Appl. Phys. Lett. 101 (23) (2012) 1–3.
[22] A. Karabutov, N. Podymova, Quantitative analysis of the influence of voids and delaminations on acoustic attenuation in CFRP composites by the laser-ultrasonic spectroscopy method, Compos. Part B: Eng. 56 (2014) 238–244.
[23] A. Karabutov, N. Podymova, Nondestructive porosity assessment of CFRP composites with spectral analysis of backscattered laser-induced ultrasonic pulses, J. Nondestr. Eval. 32 (3) (2013) 315–324.
[24] G. Wissmeyer, M.A. Pleitez, A. Rosenthal, V. Ntziachristos, Looking at sound: optoacoustics with all-optical ultrasound detection, Light Sci. Appl. 7 (1) (2018) 1–16.
[25] X. Zhang, J.R. Fincke, C.M. Wynn, M.R. Johnson, R.W. Haupt, B.W. Anthony, Full noncontact laser ultrasound: first human data, Light Sci. Appl. 8 (1) (2019) 1–11.
[26] J. Herrmann, J.-Y. Kim, L.J. Jacobs, J. Qu, J.W. Littles, M.F. Savage, Assessment of material damage in a nickel-base superalloy using nonlinear Rayleigh surface waves, J. Appl. Phys. 99 (12) (2006) 1–8.
[27] X. Jian, Y. Fan, R. Edwards, S. Dixon, Surface-breaking crack gauging with the use of laser-generated Rayleigh waves, J. Appl. Phys. 100 (6) (2006) 1–6.
[28] S. Dixon, B. Cann, D.L. Carroll, Y. Fan, R.S. Edwards, Non-linear enhancement of laser generated ultrasonic Rayleigh waves by cracks, Nondestr. Test. Eval. 23 (1) (2008) 25–34.
[29] A. Moura, A.M. Lomonosov, P. Hess, Depth evaluation of surface-breaking cracks using laser-generated transmitted Rayleigh waves, J. Appl. Phys. 103 (8) (2008) 1–6.
[30] K. Li, Z. Ma, P. Fu, S. Krishnaswamy, Quantitative evaluation of surface crack depth with a scanning laser source based on particle swarm optimization-neural network, NDT and E Int. 98 (2018) 208–214.
[31] H. Cho, S. Ogawa, M.J.N. Takemoto, E. International, Non-contact laser ultrasonics for detecting subsurface lateral defects, NDT & E International, 29(5) (1996) 301-306.
[32] C. Wang, A. Sun, X. Yang, B.F. Ju, Y.J. Pan, Laser-generated Rayleigh wave for width gauging of subsurface lateral rectangular defects, J. Appl. Phys. 124 (6) (2018) 1–7.
[33] M. Khosroshahi, M. Hadavi, M. Mahmoodi, In situ monitoring the pulse CO_2 laser interaction with 316-L stainless steel using acoustical signals and plasma analysis, Appl. Surf. Sci. 256 (24) (2010) 7421–7427.
[34] A. Kromine, P. Fomitchov, S. Krishnaswamy, J. Achenbach, Laser ultrasonic detection of surface breaking discontinuities: scanning laser source technique, Mater. Eval. 58 (2) (2000) 173–177.
[35] I. Arias, J.D. Achenbach, A model for the ultrasonic detection of surface-breaking cracks by the scanning laser source technique, Wave Motion 39 (1) (2004) 61–75.
[36] Y. Sohn, S. Krishnaswamy, Interaction of a scanning laser-generated ultrasonic line source with a surface-breaking flaw, J. Acoust. Soc. Am. 115 (1) (2004) 172–181.